SCIENTIFIC REPORTS

OPEN

SUBJECT AREAS:
RINGS AND MOONS
FLUID DYNAMICS
GIANT PLANETS
COMPUTATIONAL ASTROPHYSICS

Received
5 September 2012

Accepted
25 January 2013

Published
14 February 2013

Gravitational Vortices And Clump Formation In Saturn's F ring During An Encounter With Prometheus

Phil J. Sutton & Feodor V. Kusmartsev

Astronomy Unit, Physics department, Loughborough University, Loughborough, Leicestershire, LE11 3TU, UK.

Correspondence and requests for materials should be addressed to P.J.S. (p.j.sutton@lboro.ac.uk)

Saturn rings are most beautiful and dynamic places in the solar system, consisting of ice particles in a constant battle between the gravitational forces of Saturn and its many moons. Fan, spiral, propellers, moonlets and streamer-channels observed by CASSINI in the F-ring have been attributed to encounters by Prometheus on the F ring, with investigations of optical thickness revealing large populations of transient moonlets. Taking into account gravitational interaction between particles and a multi-stranded F-ring structure we show that Prometheus' encounters create rotational flows, like atmospheric vortices and the self-gravity enhances the accelerated growth and size of moonlets. Vortex patches form caustics, which is a primary cause of the transient particle density clumps of 20 km width and 100 km length, and they are elongated to cover an area of 1600 km by 150 km, which may eventually combine into a vortex sheet.

Detailed analysis of CASSINI observations investigating the long term evolution of streamer-channels created by Prometheus revealed fan structures at channel edges[1], including the spiral nature of the transient strands[2]. Many of the observations have already been explained and contained in previously published papers[1–8]. The basic mechanism of the streamer-channel formations has been described in detail by Murray et al.[3] using three-strands (core + 2 strands) plus a background population model. That paper included direct comparisons with Cassini images for similar configurations. Following very important results obtained by Charnoz et al.[2], where a discovery that the transient (non-core) strands were spiral in nature, has been made and by Murray et al.[4] shown on how strands formed from sheared jets produced by physical collisions, it became clear that the F ring consists of a long-lasting core with transient strands. Very important findings have been made recently by Beurle et al.[1] who have shown how Prometheus' passage causes density enhancements in the core of the F ring. Cassini images showed evidence of density enhancements in the core and the strands, as well as the connection between embodied objects producing the "fan" structures, their location at channel edges and subsequent link to Prometheus as a source of moonlet formation in the F ring. In the images there is also a puzzle in the observation of a bias in the fan structures and subsequent embodies objects being located on one side of the channel edges (here on the edge facing towards Prometheus after an encounter)[1]. However, until now there has been no explanation given for the observed bias. Furthermore, in the Ref. 1 it was shown that (i) the density enhancement is a natural consequence of the Prometheus encounter, (ii) it is reaching a maximum several orbital periods after the encounter and (iii) rises to a value ~2.5 to 3 times that of the pre-Prometheus encounter value. All these results were obtained based on a combination of Cassini observations and modeling without the use of self-gravity and inter-particle collisions. This issue is now to investigate how the gravitational interaction between particles may influence the observed phenomena and in particular, moonlet formation.

Here we describe a numerical simulation model of self-gravitating particles of the F ring in close interaction with Prometheus and Saturn, see Figure 1, which illustrates the system under study. The insert on this Figure demonstrates the relative movement of Prometheus towards the F ring, which creates periodic gravitational perturbations. It is indicated by a spiral curve. The numerical simulations[9] have proven the importance of self-gravitating particles in Saturn's rings. It was shown there that the gravitational interaction between particles has a significant effect on the shape and evolution of structures formed in the presence of embedded moonlets[9]. Therefore, it is natural to assume that the gravitational interaction between particles is important for all aspects of particle dynamics in Saturn's rings. Previous numerical modelling of the F ring used a homogeneous ring (no strands) together with analysis of CASSINI data and showed that particle number densities increasing at channel edges was a direct result of the Prometheus encounter[4]. Moreover some of these high density clumps were stable, i.e. they were capable of surviving long enough for a second pass of Prometheus, 110 orbital periods later[4]. These

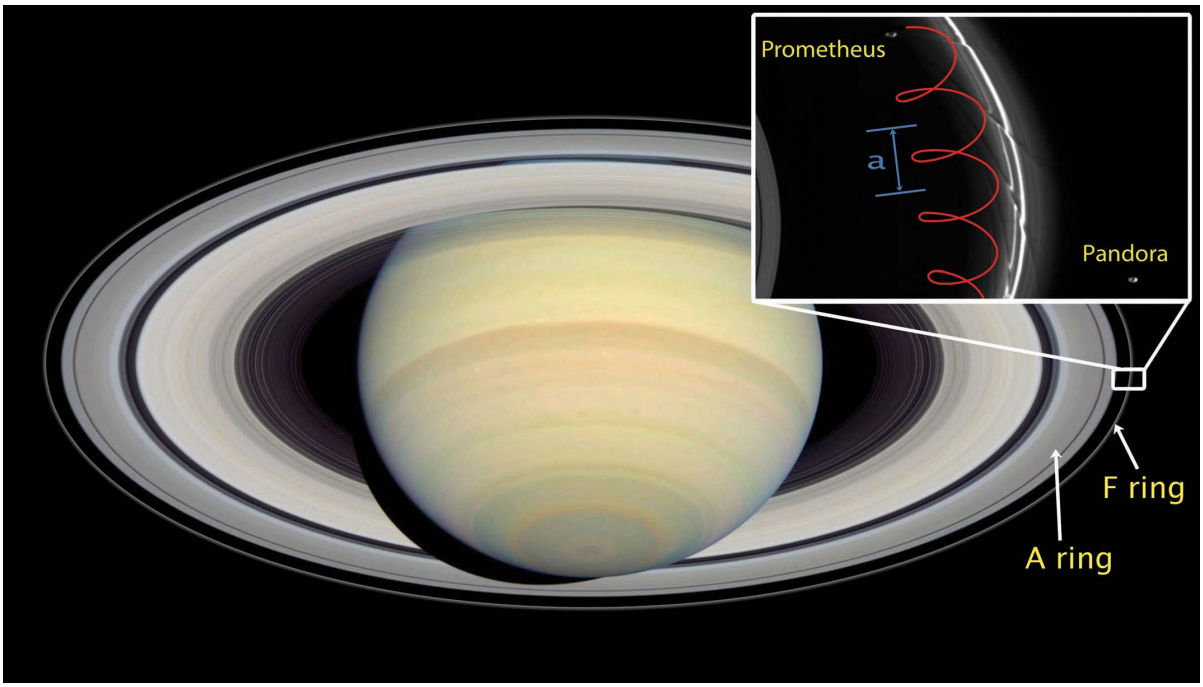

Figure 1 | How Prometheus creates structure in the F ring. The F ring is the outer most of Saturn's dense rings, located just beyond the A ring. The two shepherd moons, Prometheus and Pandora are responsible for its narrow structure of only a few hundred km. Prometheus, the larger of the two resides in the Roche Division between the A ring and the F ring. Prometheus' orbital motion: the elliptical nature of its orbit takes Prometheus towards and back away from the F ring during the course of one orbital period. Assuming a rotating reference frame that matches that of the F ring, the red line represents the trajectory of Prometheus' motion relative to the F ring. Prometheus orbits faster than particles in the F ring: in one orbital period it advances on the distance ***a***, this spacing is always 3.27°. On each approach of Prometheus structures are formed within the F ring, which is distorted over time by Keplerian shear. Due to the faintness of the F ring compared to other rings, the F ring has been drawn on the image of Saturn to represent its position in the rings. Original images from ESA/Hubble and CASSINI, image has been altered to show the location of the faint F ring outside the main visible rings imaged by Hubble. The close up image of the F ring and the shepherd moons, taken by CASSINI has been altered to show the relative movement of Prometheus to a stationary F ring.

clumps, subjected to a second Prometheus encounter, could cause a new structure formation, facilitating either the further collapse or a total destruction of the clump. Currently many mechanisms exist for the formation of moonlets and satellites in Saturn's rings[4,10,11]. However we propose a new mechanism that can be applied to Saturn's F ring. The similar idea has been used to describe planetesimal formation in Protoplanetary disks[12,13].

Our many-body numerical simulations of the F-ring dynamics, taking into account the gravitational forces from Saturn, Prometheus and between particles of the F-ring show that the Prometheus encounter is a main driving force in the formation of the rotational vortex flows observed in the analysis of our numerical simulations (see, Figure 2 + 3). We also found that self-gravitation between particles plays an important role in the growth rate of the moonlets formation. Moreover we show that the size of moonlets created in these rotational vortex flows is strongly correlated with the gravitational interaction between the F-ring particles. A new mechanism is offered for the rapid growth of metre to kilometre size moonlets in the F-ring alongside gravitational instabilities that has previously been discussed. The gravitational interaction between particles provides fluid like properties to the F-ring, and, therefore, presents an opportunity to witness first-hand the properties of an astrophysical fluid in the case of Saturn's F ring. The formations of vortices, other fluid-like excitations, fast growth rate and size of the associated moonlets, described here can be seen like some proposed processes of planetesimal formation in the Protoplanetary disk. It has already been shown that vortices greatly accelerate planetesimal formations in Protoplanetary discs[12,13], where they concentrate dust particles towards their centres, giving rise to an accelerated growth of metre to kilometre sized planetesimals compared to those formed by gravitational instabilities alone. Therewith we are offering a mechanism that could help work against the strong tidal forces known to exist in the F ring and rapidly spawn a new moonlet. We found that all stages of the streamer-channel formation and associated structures described may be identified in the CASSINI observations. Our results are also in agreement with other work done on such encounters[1–4]. However, the creation of gravitational vortices accompanying the streamer-channel dynamics and their subsequent role in moonlet formation has so far not been discussed. It is therefore important when considering the time scales involved for moonlet formation in the F ring to take into account self-gravity, and may go some way to explain the reason for such a large population of metre to kilometre sized moonlets responsible for the mini jet formations witnessed by CASSINI and already known to exist in the F ring[14].

Results

Gravitational vortices. By the term "gravitational vortex" referred to throughout the text we have in mind a new phenomenon which can exist in Saturn's rings. This is an anti-cyclonic rotational vortex flow of particles created by Prometheus during its close encounters. We have found this flow by the analysis of our numerical data obtained in extensive numerical simulations, where 6.5 million interacting particles have been considered. Here we have generated plots for the velocity vector field and associated streamline contour plots in a rotating reference frame orbiting around Saturn and keeping the average F-ring particles stationary. All plots were generated by subtracting the net orbital velocity vectors of the rotating frame from the velocity vectors of each ring particle. In both models we do not see the creation of any cyclonic vortices only anti-cyclonic

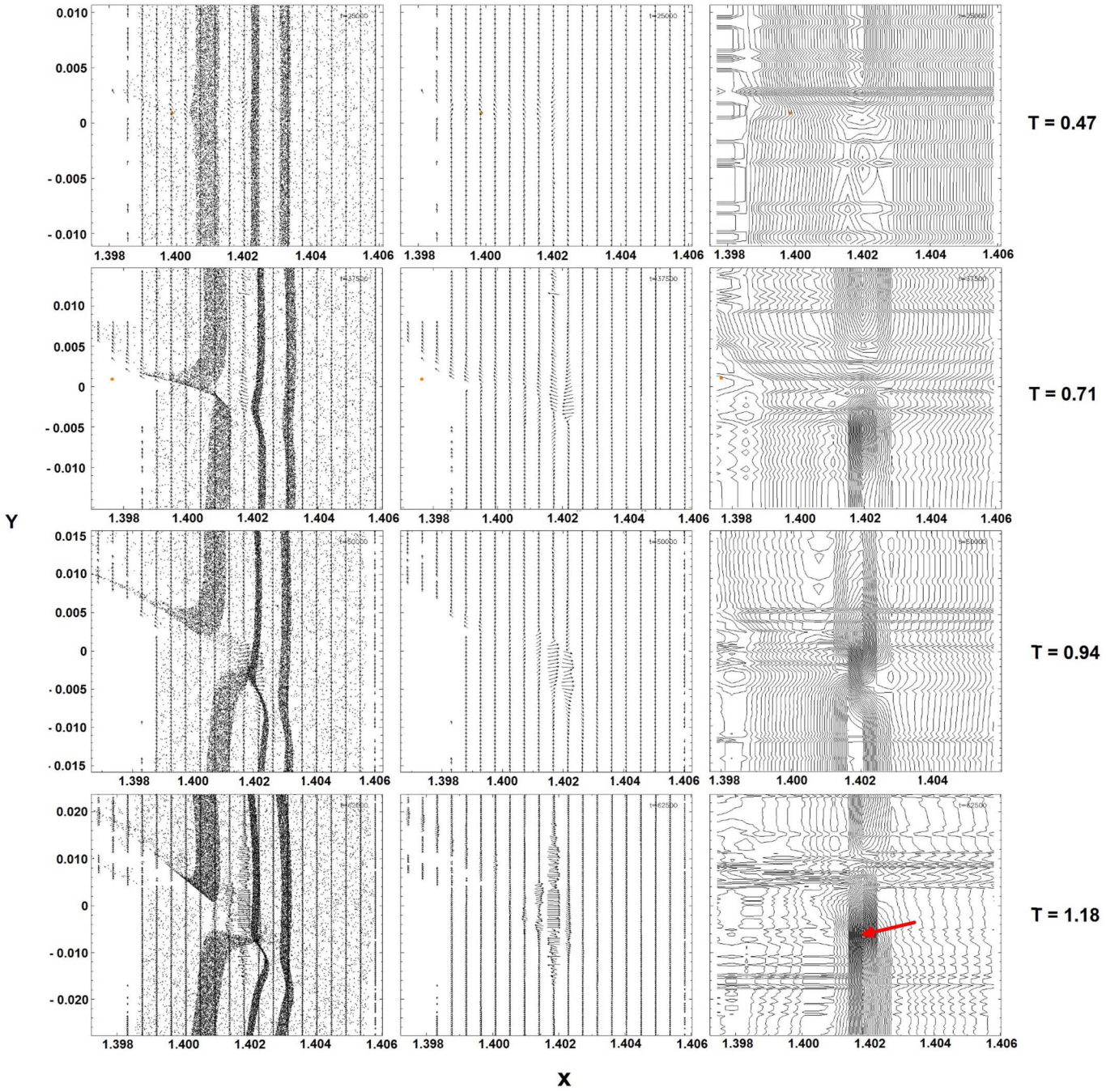

Figure 2 | The particle distribution, the velocity vector and streamline contour plots obtained in the framework of non-interacting model. Here we have taken four different time snapshots describing the formation of the particle flows within the F ring during the initial encounter of Prometheus, taken at the time: T = 0.47, T = 0.71, T = 0.94 and T = 1.18. Here for each moment of time we present the snapshot of: 1) the velocity vector plot in a rotating frame, which is shown overlaid onto the particle positions (on the left); 2) the plot of the velocity vector field without particle positions (in the centre) and 3) the streamline contour plots of the velocity vectors (on the right). Here T represents time in the model since the start in Prometheus orbital periods and both the X and Y axis scales are in 10^5 km. The red arrow identifies the centre of rotation from the streamline contour plot.

ones, see, Figs 2 and 3. A comparison of the snapshots taken during the ignition of the rotational particle flows calculated in the framework of these two (non- and interacting) models (see, Fig. 2 and 3, respectively) shows a distinct difference between them. Although up until one orbital period after the start of the numerical simulation there arises little difference between the size and structure of the disturbed velocity vectors. Then, due to a gravitational interaction between these nearest particles a distinct divergence between the snapshots of the two models emerges.

In this divergence, first, we see that the results from the non-interacting model show a larger dispersion of the disturbed velocity vectors. Each particle has its own trajectory independent from one another. The particle's trajectories diverge from each other with time revealing the individualistic nature of their orbits. This divergence appears after one orbital Prometheus period as approximately 3200 km × 150 km in size, and continues to expand as the system evolves. Second we see in Fig. 3 that at a time T = 1.18 obtained with the help of the interacting particle's model there arises a clear centre of rotation, indicated by the arrow on the snapshot: the particle

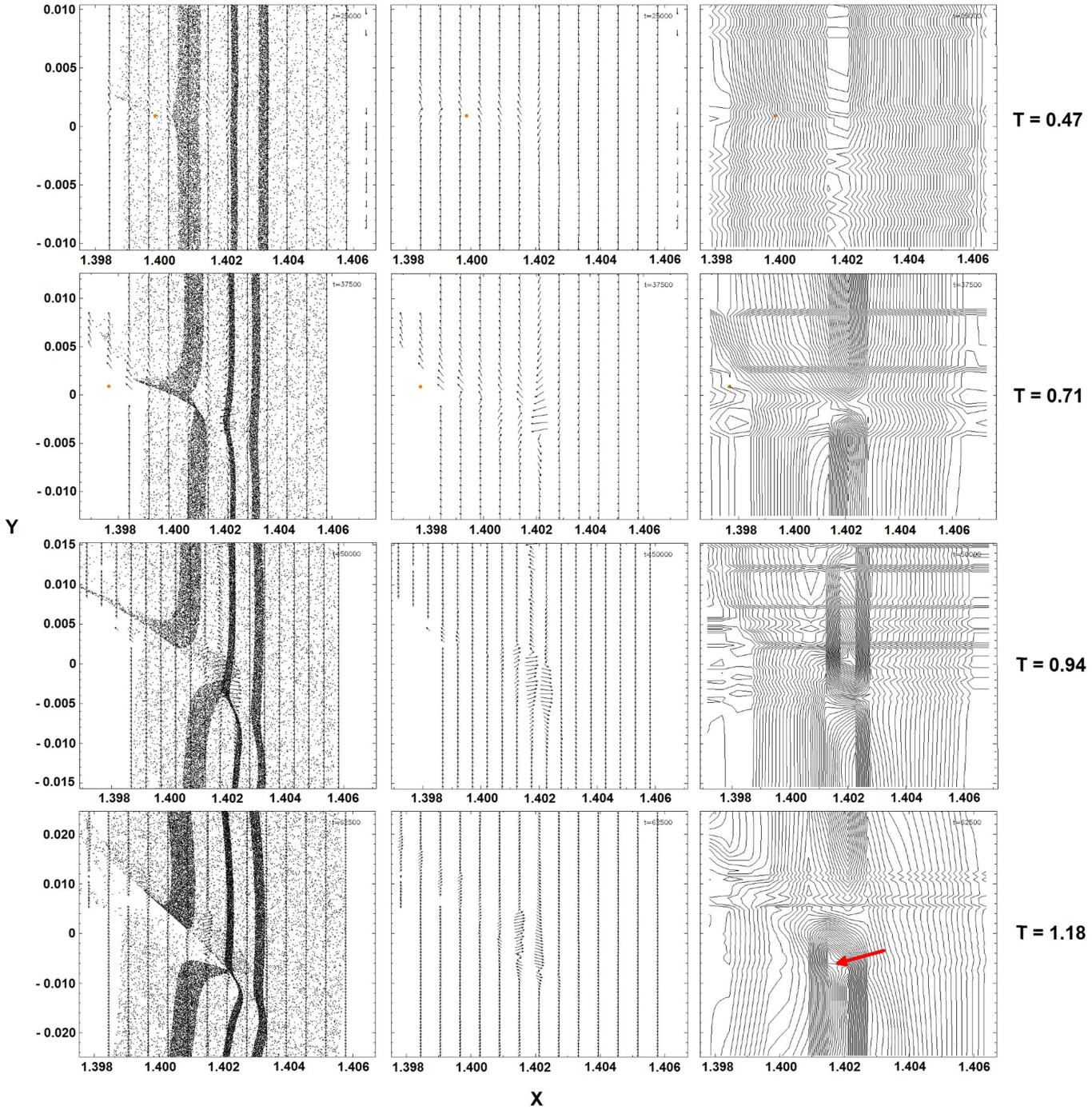

Figure 3 | The particle distribution, the velocity vector and streamline contour plots obtained in the framework of model for gravitationally interacting particles. Here we have taken four different time snapshots describing the formation of the rotational vortex flow within the F ring during the initial encounter of Prometheus, taken at the time: T = 0.47, T = 0.71, T = 0.94 and T = 1.18. For each time the snapshot (on the left) the velocity vector plot in a rotating frame is shown overlaid onto the particle positions, (on the centre) the velocity vector plot without particle positions and (on the right) the streamline contour plots of the velocity vectors. Here T represents time in the model since the start in Prometheus orbital periods and both the X and Y axis scales are in 10^5 km. The red arrow identifies the centre of rotation from the streamline contour plot.

trajectories show little dispersion from this common centre of rotation, presenting a coherent structure that is evidently more compactly bound. This is in strong contrast with trajectories obtained by means of the non-interacting model. After one Prometheus orbital period an approximate size of the rotational flow covers 1600 km × 150 km, it is approximately half the area of the non-interacting particle's flow obtained in the first model. Such strong differences once more emphasizes an important role of gravitational interaction between particle in the F ring dynamics. Third, we note that there are two distinct rotational flows appear when there are gravitational interactions between all particles. These two flows, both anti-cyclonic in nature and positioned in our figures above and then below Prometheus' position in the Y axis. The centres of these rotational flows are indicated by the arrows on the snapshots taken at the time T = 0.71. The rate of evolution for these two flows is different. The rotational flow formed near the channel edge, which faces towards Prometheus, after initial creation quickly evolves into a single coherent vortex getting stronger due to absorbing other nearby

rotations. It is also associated with a strong enhancement of the particle density at this channel edge, which is now completely involved in the rotational flow.

All flows described by both models show evidence of the destructive forces of Keplerian shear by a formation of their elongated structures. However, only the compact vortex flow created due to a gravitational interaction between particles is showing a resistance to this force. This again indicates the important role of the gravitational interaction in the vortex stability and dynamics.

The reason why we see a more chaotic or less structured rotational flow in the non-interacting model is primarily down to the fact that here all ring particles move only under the influence of two strong forces , from Saturn and Prometheus. There are no additional forces from other ring particles that could induce a fluid like motion within the ring. Instead, particles move on their own individual orbits initiated after the original encounter of Prometheus. These individual trajectories are then quickly deformed by Keplerian shear that meets no collective resistance from other particles. On the contrary we see the opposite trend for rotational flows obtained in the interacting model where all ring particles are influenced by the movement of other ring particles. A special role here is played by clumps or areas of the enhanced density since they have a larger mass and consequently a stronger gravitational influence on other particles. Here we see the formation of a coherent structure where collectively particle velocity vectors combine to form a defined rotational flow that we hereby refer to as gravitational vortices. Thus, we see in Figure 3 that after the F ring encounters Prometheus a rotational vortex motion arises. The vortex core is dispersed and is always located on the channel edge facing towards Prometheus after the initial encounter.

Indeed it has been observed by CASSINI and noticed in the analysis of the CASSINI observations by Beurle et al[4] that the formation of moonlets by Prometheus would favour one channel edge over the other. In this case the edge facing towards Prometheus. This is consistent with our results where we found that the gravitational vortex is formed exactly on the same edge of the channel. Therefore, we believe that we have found a mechanism for the asymmetry or "bias" observed in Ref. 4.

The gravitational vortex behaviour and position in the F ring is determined by Prometheus encountering the F-ring on its faster orbit relative to the F ring. The geometry of their mutual motion dictates the breaking of the symmetry between the left and right hand edges of the channel. If we imagine that Prometheus would reverse its relative motion there will be formed an anti-vortex (cyclonic), vortices and ensuing clumps would now favour the opposite channel edge. So the gravitational vortex is formed due to self-gravity that increases the density around the vortex core. This density enhancement may lead to an increase in local density or even to the formation of a moonlet.

This then is reminiscent of planetesimal formations seen in a proto-planetary system[8] or a spiral micro-galaxy. The trajectories of the gravitational vortex also create a caustic of the closed particle trajectories and associated new high-density clumps when the vortex drifts between the strands. Especially it is clearly seen when it is approaching the dense inner strand of the ring. With time many gravitational vortices may be created, and we may speculate that under the strong tidal forces seen in the F ring these vortices may elongate and join other adjacent vortices leading to a formation of various structures as, for example, a vortex sheet[15–17].

Density distribution in the F ring. We have carried out an in depth analysis of the density distributions in the F ring by calculating number densities in a square box with sides 1000 km surrounding each of the areas identified in Fig. 4. The particle number density is defined as the number of nearest neighbours of the host particle within a certain distance from this particle. In our calculations we have chosen this distance to be 2 km. Then we define the density distribution of particles as the number of particles having a particular number density. Following these definitions then the number of nearest neighbours within a 2 km radius of each particle in the box boundary (1000 km $\times$ 1000 km) has been calculated. We are particularly focusing on the maximum number density and the density distribution in each of the clumps identified in the Fig. 4. Below we provide also comparative quantitative values for the density distributions obtained within the two models studied of non- and interacting particles, respectively (Table 1).

What we note is that the highest value for the density is seen in both models was in region i). This region is on the channel edge facing towards Prometheus on the inner strand formed after one orbit after its initial encounter. For gravitationally interacting particles during subsequent orbits the maximum density at the channel edge in the central core first drops by 37.5% compared with that seen on the inner strand previously. However we see approximately 5% density increase in each orbit thereafter. In all cases we observe a general trend showing an upwards growth in density for each region as the system evolves after the initial encounter by Prometheus. Here the density profile of each region obtained within the interacting particles model (see, supplementary Fig. s4) shows that although the maximum number density does not change by a large amount after each orbit the profile of the density shifts upwards. Therewith we are demonstrating that with time more particles are exhibiting a higher number density in the same region. Therefore, it is showing that the local density in the clumps increases as the system evolves. In this gravitational accretion processes the self-gravity is creating a larger area growing with the time where particles have a higher local density than the rest of the un-perturbed F ring.

We found, see the Table 1 that in the model describing non-interacting particles the maximum number density in the region identified as a clump in Fig. 4a does not show evidence of any increase. In fact, even a decrease is seen in some of the locations, see Fig. 4a. This is consistent with the numerical results obtained by Beurle et al (2010)[4] for a model of non-interacting particles on non-stranded ring. There, an increase in the maximum number density for the first 5 orbits was also not observed. Not only this but also the clump density profiles (see, Fig. s3, in supplementary material) show that the majority of particles have on average a much lower number density.

On the other hand the results obtained with the use of the model of self-interacting particles are very different; see the second column in the Table 1. The difference in the results obtained with the use of these two models (associated with two columns in the Table 1) is especially clearly seen for the maximum number density taken after the first 5 orbits. It develops into a value of 20% – 35% for comparable regions after only a short period of time. Again this strong difference between the densities calculated with the use of non- and interacting particle models further supports the argument for an accelerated growth rate of moonlets driven by gravitational interaction between particles.

When comparing the results obtained with the use of these two models the most notable feature seen is the change in density distribution profile in each region. Although in the case of interacting particles the maximum clump density shows a relatively small increase after each Prometheus orbit we note that the biggest transformation arises in its density profile. We see that more particles in the clump have on average a higher number density. This suggests that the clumps are growing faster and to larger size when self-gravity is taken into account. This is, therewith, preventing the same regions from dispersing during the orbital fluctuations.

Comparison with CASSINI images. A comparison between CASSINI images and our data is shown in Fig. 5. An image captured by CASSINI in July 2009 when Prometheus and the F ring were close to their minimum separation due to precession in their respective elliptical orbits is shown in Fig. 5a. Fig. 5b shows how

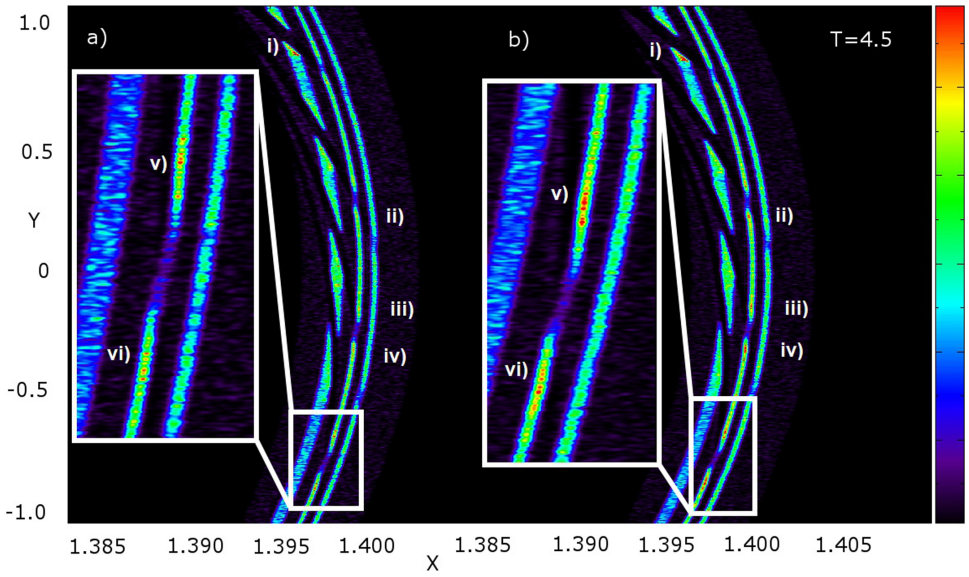

Figure 4 | The density distributions obtained with the use of the models of non-interacting and interacting particles. Two snapshots in the density distribution, (a) and (b), obtained with non-interacting massless particles and interacting particles models. The particles mass is m = 10 kg. Both snapshots are taken at the same time, T = 4.5, after the initial Prometheus encounter where T is the number of orbital periods since the beginning of the numerical simulation and where Prometheus started at the periapsis of its orbit. To make a comparison between the results obtained within these two models we have chosen six regions of the F-ring noted as i)–vi), where the density distribution has a strong variation due to a formation of channels. Channels are orientated from youngest, at the top of the figure to oldest at the bottom of the figure. The Prometheus is effectively moving from the bottom upwards in relation to the F ring in a rotating reference frame. (a) The snapshot of the density plot obtained with the use of the non-interacting particles model, here only a very modest increase in the local density is seen. The density has a maximal enhancement at the channel edges, with the most seen at those edges in the central core. (b) The snapshot of the density plot obtained with gravitationally interacting particles model. Here we see a much faster increase in local density, which is more enhanced at the channel edges in the central core. By the fourth channel, shown by the zoomed section we can see that the local density increases on both edges that shows considerably greater values than those at the same time and position obtained within the non-interacting particles model. The areas (a) i)-iv) and (b) i) – iv) in the density distribution obtained within these two models have shown a similar difference in the density profile. To make a more solid conclusion about an important role of gravitational interaction in the clump formation we have performed a more depth analysis of their density profiles below presented in Figures s3 and s4 of the supplementary material.

the particles are distributed in the F ring in our numerical model after Prometheus makes a close encounter, inducing the formation of a streamer. Distribution of density at the same snapshot in time is shown in Fig. 5c. An area in the centre of the ring at the opposite end of the streamer pointing to Prometheus is the high density clump created due to the movement of inner strand particles into the central F ring core. When analysed, the CASSINI image (Fig. 5a) shows an average brightening (marked by red box) compared to the overall brightness to the rest of the strand of ~26%, compared to an average increase in number density in the same area of 25% in our models. This is noted as being of the same formation as mentioned previously in the region i) of Fig. 4, but at a slightly earlier time of its evolution. So we have shown that the strongest density perturbation is occurring during the initial encounter and is effectively the result of an overlapping of the inner strand and central core.

Table 1 | We show here the maximum value of the density measured in each of the regions identified in Fig. 3. Where, the value T = 0 corresponds to the initial density of the same region at the start of the simulation prior to any perturbation of Prometheus

Region	Max No. Density (Non-interacting)	Max No. Density (Interacting)
T = 0	16	16
i)	27	32
ii)	19	20
iii)	17	21
iv)	19	22
v)	17	23
vi)	19	23

Discussion

Our simulations indicate that such density clumps are transient in nature; their growth rate and their life time depend on the self-gravity of particles and are associated with rotational vortex flow. Obviously, such complex dynamics is due to the gravitational forces between particles and original gravitational vortex flows, because Prometheus is already on a far enough distance and has a weak gravitational influence on the events. The vortices continue to play a vital role in density fluctuations when Prometheus is no longer the primary cause of disruption within the F ring. As a result of the gravitational collapse and the rotational flow, an area of enhanced density forms in the central F ring core as particles from the two strands come together, creating an area of increased density ~100 km by 20 km (see, supplementary Fig. s1e). This clump exists for a longer time than just one orbital Prometheus period. Of course the gravitational forces between particles when self-gravity is taken into account keep them together if density exceeds that of the local Roche density for the F ring. The density of clumps regularly and periodically fluctuates on the strands and core forming a non-linear density wave, through their internal movement within the gravitational vortex. Thus, we see that the advances and retreats of Prometheus from the F ring stimulates rotational vortex motion of ring particles, visible well known streamer-channels[2–4] as well as exciting non-linear density waves on the inner strands. Our modelling provides many new details in the variation of encounters due to the precession in offset between the elliptical orbit of Prometheus and that of the F ring. However, the most interesting occurs only when these two are at minimum

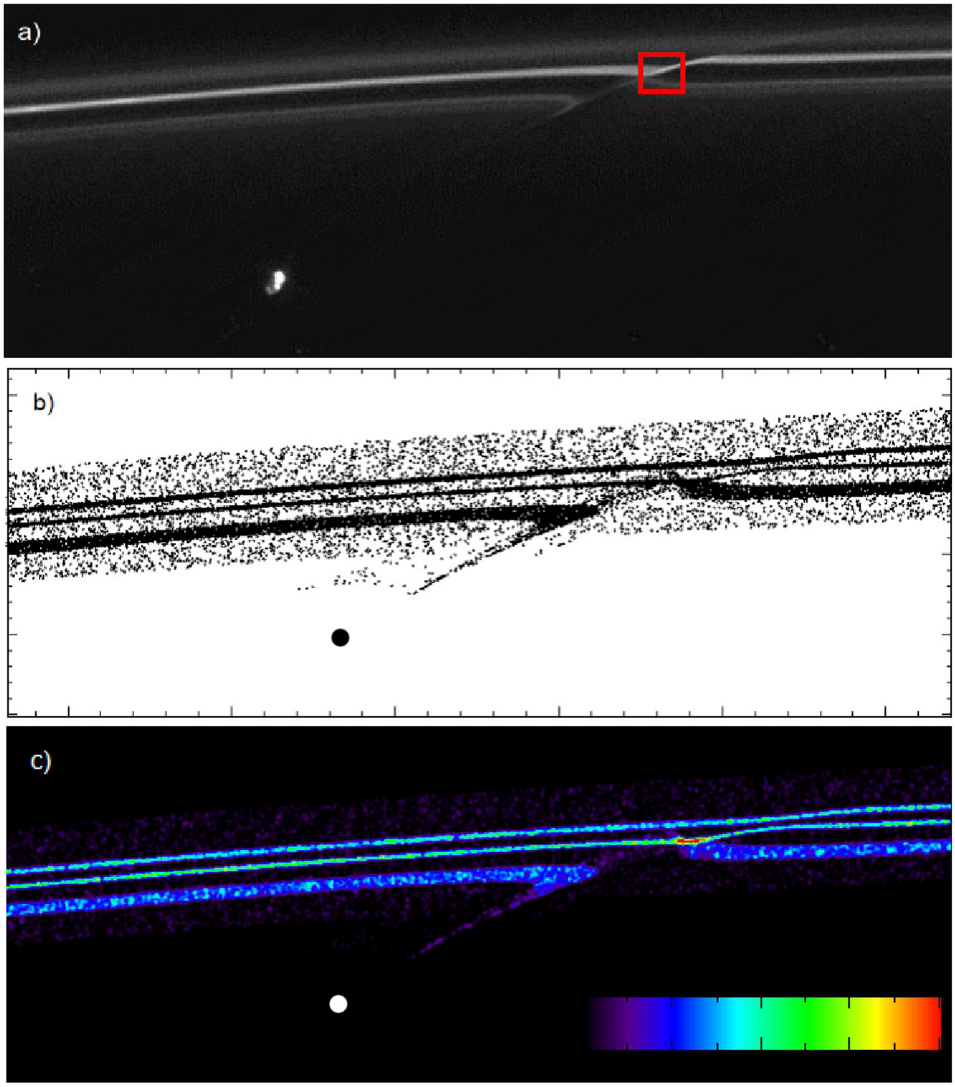

Figure 5 | Comparison between CASSINI observations and our numerical model. For this configuration Prometheus has a mean anomaly of 312°. The difference in position of Prometheus in our models is down to a slightly different viewing angle than those taken with CASSINI which was not taken directly above. Prometheus is shown as the bold white/black circle in our models. (a) Image taken by CASSINI, image ID: 1_N1627542144.118 and date and time of mid exposure of 2009-07-29, 06 : 20 : 22.5, this is near when Prometheus' orbit is aligned so that it makes its closest approaches to the F ring. The red square identifies the area in the CASSINI image that corresponds to an increase in density seen in our model. (b) A snapshot taken of our model showing the same position in Prometheus' orbit. The frame is rotated to match observations made by CASSINI at the time. (c) A plot of particle number density is done for the same frame as (b).

separation, it is a formation of the gravitational vortex flow covering an area of 1600 km by 150 km. A larger less coherent flow is seen for the non-interacting flow witnessed in our models. The moon's clashes with the F-ring have been recorded by CASSINI in December 2009 where the F ring and Prometheus orbits have been aligned for their most extreme approach. It is likely that during that time the described gravitational vortex can be created. Again here we note that this is also dependant on the longitudinal position of the transient strands at the time of encountering. But it is only at minimum separation that a splitting of the inner strand and subsequent overlapping of the core is likely to occur. Regardless of the longitudinal position of strands, the gravitational vortices behaviour and creation are dependent on separation between the F ring and Prometheus. We believe that the probability of their occurrences is greatly reduced at any larger separations and alignments.

We can therefore assume that if the clumps density exceeds the local Roche density then further gravitational collapse is possible. The self-gravity is greatly increasing the life time of any clumps in general as we seen in our simulations. CASSINI has already provided evidence that localised condensations can create[2–9] embedded objects, which can also go on to live long enough to create various structures in the F ring. The many-body dynamics of a narrow ring of particles being perturbed by a moon studied here may be also applicable to a description of the planetesimal formation in a Protoplanetary disc[12]. Prometheus creates a rich dynamical system in the F ring. The original perturbation by Prometheus creates a vortex flow, facilitating the formation of smaller moonlets that they themselves go on to generate their own structures in the form of fans, spirals and jets. We also believe that in cases where vortices are long lived they can be responsible for the brightening seen in the F ring[18]. It occurs when Prometheus' orbit was aligned with the F ring.

The density enhancement obtained in our simulations of the F-ring, consisting of 6.5 million self-gravitating particles, generally agrees well with those seen in observations by Beurle et al[4] when looking at the time evolution of density seen at the channel edges. However, in the obtained density distributions there is a striking

difference with all previous work which was based on studies of non-self-gravitating particles (see, Refs1,4 and references therein). The point is that in our modelling of the F ring we have included a stranded structure and that seems very important when we consider self-gravitating particles. By including these strands and the self-gravity in our model, we found that the density variation, which originated due to the first Prometheus encounter of the F-ring, has reached a maximal value significantly faster compared to those seen at the channel edges over multiple orbital periods of Prometheus estimated within simpler models. This effect of the fast growth of moonlets arises mainly due to the many-body interaction of these self-gravitating particles and the stranded structure of the F-ring. The close encounter of Prometheus causes an overlap of the inner strand and central core which resulted in a large increase in the local density over a very short time period. This is comparable to those shown in Fig. 5 at channel edges. However, in our simplified stranded model, it is only when the F ring and Prometheus are aligned at minimum separation, does the inner strand distort enough to overlap into the central core, giving rise to the largest increase in density.

When comparing the two models, non-interacting and interacting particles, we found that it is very important to consider F ring particles with an appropriate mass. The self-gravity plays a very important role in the density enhancement. It significantly accelerates the growth rate of large clumps. This can be shown with a 20%–35% increase maximum number density in clumps seen at channel edges for our interacting model compared with the non-interacting model. On-going observations of CASSINI continue to offer great insight into of one of the most dynamic and interesting systems in the Solar System where self-gravitating ring particles are in a constant battle creating gravitational vortex flows, high density clumps and their collapses.

Methods

To obtain the results in our manuscript we employed an n-body simulation of 6.5×10^6 point like particles where they evolved in the system due to gravitational forces taken from classical Newtonian mechanics[19]. The equations of motion for each particle as well as for Prometheus and Saturn can be shown as:

$$\ddot{\vec{r}}_s = -G\sum_{i=1}^{N}(\vec{r}_i-\vec{r}_s)\frac{M_i}{|\vec{r}_i-\vec{r}_s|^3} - G(\vec{r}_p-\vec{r}_s)\frac{M_p}{|\vec{r}_p-\vec{r}_s|^3} \quad (1)$$

$$\ddot{\vec{r}}_p = -G\sum_{i=1}^{N}(\vec{r}_i-\vec{r}_p)\frac{M_i}{|\vec{r}_i-\vec{r}_p|^3} - G(\vec{r}_s-\vec{r}_p)\frac{M_s}{|\vec{r}_s-\vec{r}_p|^3} \quad (2)$$

$$\ddot{\vec{r}}_I = G\sum_{J\neq 1}^{N}(\vec{r}_I-\vec{r}_J)\frac{M_j}{|\vec{r}_I-\vec{r}_J|^3} - G(\vec{r}_p-\vec{r}_I)\frac{M_p}{|\vec{r}_p-\vec{r}_I|^3} - G(\vec{r}_s-\vec{r}_I)\frac{M_s}{|\vec{r}_s-\vec{r}_I|^3} \quad (3)$$

The numerical simulation started with Prometheus at the periapsis of its orbit, with no accelerations being assigned to particles in the initial conditions. Two separate numerical models were created, both assuming 6.5×10^6 point-like particles with no physical size. The first model assumed all ring particles to be massless test particles moving only under the influence of Saturn and Prometheus. The second model assumed a single ring particle mass of 10 kg whose motion is influenced not only by Saturn and Prometheus but also every other particle in the F ring. When creating the starting position of particles we used parameters previously used for numerical modelling of the F ring[1], strands and the central core. To create a more realistic F ring structure all ring particles were arranged randomly into four groups or rings around Saturn, with the first being a background sheet of particles and the subsequent three groups being the inner strand, central core and outer strand respectively. The central core contained 2×10^6 particles to account for the suspected higher particle densities that are present in the core. The inner strand, outer strand and background population group all contained 1.5×10^6 particles each, distributed randomly with equal probability around the whole ring. The strands and core were all assumed not to be spiral in nature for the sake of our modelling were the true trajectories of particles within these strands can be difficult to model. These distributions are associated with the initial conditions of the particles used in our numerical modelling. They automatically give rise to a higher particle number densities in the inner and outer strand and higher again in the central core. This choice has been based on the observations made by CASSINI, which have suggested a higher density in a central core and strands (assuming a higher surface brightness). The reference frame has been chosen with Saturn placed at the origin of our system of coordinates, where its initial conditions were associated with a zero magnitude velocity vector. Therefore the equations for initial positions of all particles can be shown as:

$$\vec{R_s} = [0,\ 0,\ 0] \quad (4)$$

$$\vec{R_p} = [139{,}671\ km,\ 0,\ 0] \quad (5)$$

$$\vec{R_J} = [r * \cos\theta, r * \sin\theta,\ 0] \quad (6)$$

Where r represents the radial position of ring particles from Saturn and θ the angular position of ring particles around Saturn. All ring particles are assumed to have circular-like trajectories located within the F-ring; this has been done to help with creating figures that have multiple stages of evolution with respect to orbital periods since the beginning of the numerical model. The initial positions for the radial distances of particles from Saturn are split into four groups or rings to represent the background sheet of particles, inner strand, central core and outer strand respectively.

$$r(0:1{,}499{,}998) = r_1 + w_1 * random(n_1) \quad (7)$$

$$r(1{,}499{,}999:3{,}499{,}998) = r_2 + w_w * random(n_2) \quad (8)$$

$$r(3{,}499{,}999:4{,}999{,}998) = r_3 + w_3 * random(n_1) \quad (9)$$

$$r(4{,}499{,}998:6{,}499{,}999) = r_4 + w_4 * random(n_1) \quad (10)$$

Where the number inside the brackets represents particle ID belonging to each of the four groups. The values r_1, r_2, r_3, r_4 are the radial distances from Saturn to the inner ring boundary for each of the four ring groups, w_1, w_2, w_3, w_4 are the widths of each ring and the function *"random(n)"* represents a random number generated from 0.000 to 0.999 $n_1(1{,}500{,}000)$ or $n_2(2{,}000{,}000)$ times.

Each ring inner boundary and width can be shown as:

$$r_1 = 139{,}876\ km \qquad w_1 = 700\ km$$

$$r_2 = 140{,}049\ km \qquad w_w = 70\ km$$

$$r_3 = 140{,}214\ km \qquad w_3 = 20\ km$$

$$r_4 = 140{,}299\ km \qquad w_4 = 30\ km$$

An angular position θ for each of all ring articles has been taken as:

$$\theta = 2\pi * random(N-2) \quad (11)$$

Velocities of all particles in the initial conditions of our numerical modelling have been derived from equations for circular orbits, and given by the following equations:

$$\dot{\vec{R}}_s = [0,\ 0,\ 0] \quad (12)$$

$$\dot{\vec{R}}_p = [0,\ v_p,\ 0] \quad (13)$$

$$\dot{\vec{R}}_J = [v * \cos\theta,\ v * \sin\theta_v,\ 0] \quad (14)$$

Where:

$$v_p = \sqrt{\frac{\left(G(M_s+M_p)\right)(1+e)}{(1-e)*a}} \quad (15)$$

And Prometheus is assumed to be starting at the periapsis of its orbit. This condition is assumed to be the case throughout the manuscript, the parameters of its orbital are taken from Spitale et al (2006)[20].

The magnitude and angle of the initial velocity vectors of all ring particles can be expressed through the generated random numbers (see, eqs (8–12)) with the use of the formulae:

$$v = \sqrt{\frac{G(M_s+M_J)}{r}} \quad (16)$$

$$\theta_v = \theta + \frac{\pi}{2} \quad (17)$$

We used an integration method that reduced the overall computation time down significantly by using a TreePM code that was parallelised across multiple processing cores using Peano-Hilbert domain decomposition. To reduce the overall number of force calculations close range forces were computed using a Barnes–Hut Tree code whilst long range forces used a PM (particle mesh) method. Where the Particles involved in long range force calculations were grouped together with other nearby particles in a clouds-in-cells (CIC) approach with the forces calculated using a FFTW technique, see, for more details, the Ref. 19. In the TreePM method a discretized particle system is mapped into continuous model with the peculiar potential defied as:

$$\phi(x) = \sum m_i \varphi(x - x_i) \quad (18)$$

Where $\varphi(x-x_i)$ a single particle gravitational potential as is used to get gravitational forces in the equation of motion above, in eqs (1–3). Then this potential, eq. (18), is split in Fourier space into a long-range and short-range part according to $\phi_k = \phi_k^{long} + \phi_k^{short}$, where:

$$\phi_k^{long} = \phi_k \exp(-k^2 r^2) \tag{19}$$

$$\phi_k^{short} = -G \sum \frac{m_i}{r_i} erfc\left(\frac{r^i}{2r_s}\right) \tag{20}$$

Where r_s is the spatial scale of the force split.

As well as reducing down the overall force calculations carried out adaptive time stepping was used for all particles, therefore particles time steps would be derived based upon its acceleration and assigned smoothing length, see for a detail the Ref. 19. The time step of each particle can be shown as:

$$\Delta T_{grav} = min\left[\Delta t_{\max}, \left(\frac{2\eta\varepsilon}{|\alpha|}\right)^{1/2}\right] \tag{21}$$

Where Δt_{max} is the maximum allowed time step, α is the acceleration of the particle, η is the accuracy parameter, ε is the smoothing length of the particle.

No hydro-dynamical forces were included within the calculations, only the gravitational forces. We also did not include physical collisions between particles instead two particles interacting have a reduced (or smoothing) gravitational force once the distance between them became smaller than some characteristic smooth length common for all ring particle. Saturn and Prometheus have different, larger smoothing lengths, associated with their masses. The system boundaries have not been defined and so the system was open and particles can escape the ring. So, the periodic boundary conditions used in previous ring modelling have not been used here in our models.

All data created was visualised using SPLASH[21] a tool for the visualisation of SPH numerical simulations. All density plots were created using original snapshot files output from our numerical code and used a fake smoothing length assigned to each particle to create an artificial particle density which could be represented relative to all other particles in the ring. Only ring particles with the same mass were used in the creation of density plots i.e. only ring particles. To create plots showing particle velocity vectors in a rotating frame to fully illustrate the ignition of vortices the velocity arrays were modified. For each snapshot used to create the vector plots the overall orbital velocity of a rotating reference frame centred on the F ring was subtracted from the original velocity of all particles using programs written in IDL. The modified velocity vectors then showed the particle trajectories in the rotating reference without the dominating orbital velocity. Programs written in IDL were also used to calculate the maximum of the particle's number density at specific points in space and time arising at the evolution of the F-ring. By placing a box around the area of interest the particle's number density was measured and then the results obtained with the use of the two models have been compared.

1. Beurle, K. *et al.* Direct Evidence For The Gravitational Instability And Moonlet Formation In Saturn's Rings. *ApJ* **718**, L176–180 (2010).
2. Charnoz, S. *et al.* Cassini Discovers A Kinematic Spiral Ring Around Saturn. *Science* **310**, 1300–1303 (2005).
3. Murray, C. D. *et al.* How Prometheus Creates Structure In Saturn's F ring. *Nature* **437**, 1326–1329 (2005).
4. Murray, C. D. *et al.* The Determination Of The Structure Of Saturn's F ring By Nearby Moonlets. *Nature* **453**, 739–744 (2008).
5. Esposito, L., Meinke, J., Colwell, J. E., Nicholson, P. D. & Hedman, M. M. Moonlets And Clumps In Saturn's F ring. *Icarus*, **194**, 278–289 (2008).
6. Cuzzi, J. N. *et al.* An Evolving View Of Saturn's Dynamic Rings. *Science* **327**, 1470–1475 (2005).
7. Hedman, M. M. *et al.* The Christiansen Effect In Saturn's Narrow Dusty Rings And The Spectral Identification Of Clumps In The F Ring. *Icarus* **215**, 695–711 (2011)
8. Meinke, B. K., Esposito, L. W. & Sremcevic, M. Transient Clumps in Saturn's F Ring. *EPSC-DPS Joint Meeting* 2–7 October 2011 in Nantes, France, 1455 (2011).
9. Lewis, M. C. & Stewart, G. R. Features around embedded moonlets in Saturn's rings: The role of self-gravity and particle size distributions. *Icarus* **199**, 387–412 (2009).
10. Crida, A. & Charnoz, S. Formation of Regular Satellites from Ancient Massive Rings in the Solar System. *Science* **338**, 1196–1199 (2012).
11. Griv, E. & Gedalin, M. A Driving Mechanism for Moonlets Formation in Saturn's A Ring. EGU General Assembly 2010, 2–7 May, 2010 in Vienna, Austria 6281 (2010).
12. Barranco, J. A. & Marcus, P. S. Vortices In Protoplanetary Disks And The Formation Of Planetesimals. *BAAS* **33**, 1081 (2001).
13. Chang, P. & Oishi, J. S. On The Stability Of Dust-Laden Protoplanetary Vortices. *ApJ* **721**, 1593–1602 (2010).
14. Attree, N. O., Murray, C. D., Cooper, N. J. & Williams, G. A. Dection Of Low-Veloicty Collisions In Saturn's F Ring. *APJL* **755** (2012)
15. Eltsov, V. B., Blaauwgeers, R., Kopnin, N. B., Krusius, M., Ruohio, J. J., Schanen, R. & Thuneberg, E. V. Transitions From Vortex Lines To Sheets: Interplay Of Topology And Dynamics In An Anisotropic Superfluid. *Phys. Rev. Lett* **88**, 65301 (2002).
16. Hänninen, R., Blaauwgeers, R., Eltsov, V. B., Finne, A. P., Krusius, M., Thuneberg, E. V. & Volovik, G. E. Structure of the Surface Vortex Sheet between Two Rotating ^{3}He Superfluids. *Phys. Rev. Lett* **90**, 225301 (2003).
17. Bewley, G. P., Paoletti, M. S., Katepalli, R., Sreenivasan, K. R. & Lathrop, D. P. Characterization of reconnecting vortices in superfluid helium *PNAS* **105**, 13707–13710 (2008).
18. French, R. S. *et al.* The Brightening Of Saturn's F Ring. *Icarus* **1**, 181–193 (2012).
19. Springel, V. The Cosmological Simulation Code GADGET-2. *MNRAS* **364**, 1105–1134 (2005).
20. Spitale, J. N., Jacobson, R. A., Porco, C. C. & Owen, W. M. The Orbits Of Saturn's Small Satellites Derived From Combined Historic And CASSINI Imaging Observations. *ApJ* **132**, 692–710 (2006).
21. Price, D. J. Splash: An Interactive Visualisation Tool For Smoothed Particle Hydrodynamics Simulations. *PASA* **24**, 159–173 (2007).

Acknowledgements

This research has made use of data obtained by the CASSINI project from the Planetary Data System (PDS). We are very grateful to Sebastian CHARNOZ for very careful reading the manuscript and very useful suggestions, C. D. Murray for his kind clarification of the previous Saturn rings modelling where self-gravity has not been taken into account and to D. R. Gulevich for his initial help in setting up of the numerical code.

Author contributions

P.J.S. performed the numerical simulations, analysed the results and wrote the manuscript. F.V.K. contributed ideas, took part in discussions of results and helped with editing of the manuscript.

Additional information

Supplementary information accompanies this paper at http://www.nature.com/scientificreports

Competing financial interests: The authors declare no competing financial interests.

How to cite this article: Sutton, P.J. & Kusmartsev, F.V. Gravitational Vortices And Clump Formation In Saturn's F ring During An Encounter With Prometheus. *Sci. Rep.* **3**, 1276; DOI:10.1038/srep01276 (2013).